Dynamic modeling and energy analysis of renewable heating and electricity systems at residential buildings using Phase Change Material based heat storage technologies

Ioannis Violidakis, Konstantinos Atsonios, Petros Iliadis, Nikolaos Nikolopoulos

Centre for Research and Technology Hellas, Chemical Process & Energy Resources Institute (CERTH/CPERI). Athens branch: Egialias 52, GR-15125 Marousi, Athens, Greece

[*] *corresponding author: atsonios@certh.gr*

Abstract

Several heat storage systems for domestic application can be used to promote Renewable Energy Sources (RES) penetration by storing excess energy, which would otherwise be rejected during curtailments. The present study investigates two types of PV powered latent heat storage technologies for delivering heat and/or electricity at residential buildings and compares them against a reference case which uses a conventional heat pump as a heating system, also powered by a PV. One technology involves a low temperature PCM thermal energy storage system (LT-TES) heated by either an electric resistance or a heat pump and the other technology involves an ultra-high temperature TES (UHT-TES). It is revealed that any case with heat storage is preferable for better exploiting the produced renewable energy than the conventional one which does not include heat storage. The most favorable from this aspect are the cases which include the UHT-TES, which provide both heat and electricity. Focusing exclusively on heat supply, the most preferable case from a technical performance aspect is the one which includes a heat pump and a LT-TES system, albeit not providing any electricity. On the other hand, the most advantageous only in terms of electricity supply is the case which includes the UHT-TES system.

Keywords: Dynamic modeling; Dymola; RES; Phase Change Materials (PCM); Thermal Energy Storage (TES)

1 Introduction

Buildings were responsible for around 40% of EU final energy demand and for 36% of the greenhouse gas emissions in 2015 [1, 2]. There are two main strategies that aim to mitigate the impact of building sector on global warming; improvement of the energy performance of buildings reducing the energy consumptions [3] and defossilizing of the building sector, adopting renewable based solutions. As regards the first strategy, demand side management strategies and minimization of dwelling heat losses [4, 5] are the main pillars. Concerning the second strategy, the use of renewable energy for heating and cooling has been considered. Numerous studies dedicated on the combination of advanced energy systems have been performed, involving electricity-driven air conditioning equipment, mainly heat pumps, powered by photovoltaic (PV) systems [6-11]. However, the maximization of Renewable Energy Sources (RES) penetration makes the use of appropriate heat storage technologies necessary. High share of RES power capacity leads to increasing curtailment, which results in less use of wind or solar power than what is potentially available [12]. The integration of a heat storage system in a power-to-heat system may have a major contribution in mitigating curtailments during low load periods and ultimately

increasing RES utilization. The implementation of heat storage would allow for the exploitation of any excess energy which would otherwise be lost.

Towards this direction, there are several solutions for Thermal Energy Storage (TES) which can be applied in domestic level heating. Thermal energy can be stored as a change in internal energy of a material mainly as sensible heat or latent heat [13], but there are also other options in which thermochemical energy or combination of these is stored [14] (Figure 1). The most common TES systems are the ones which store sensible heat [15].

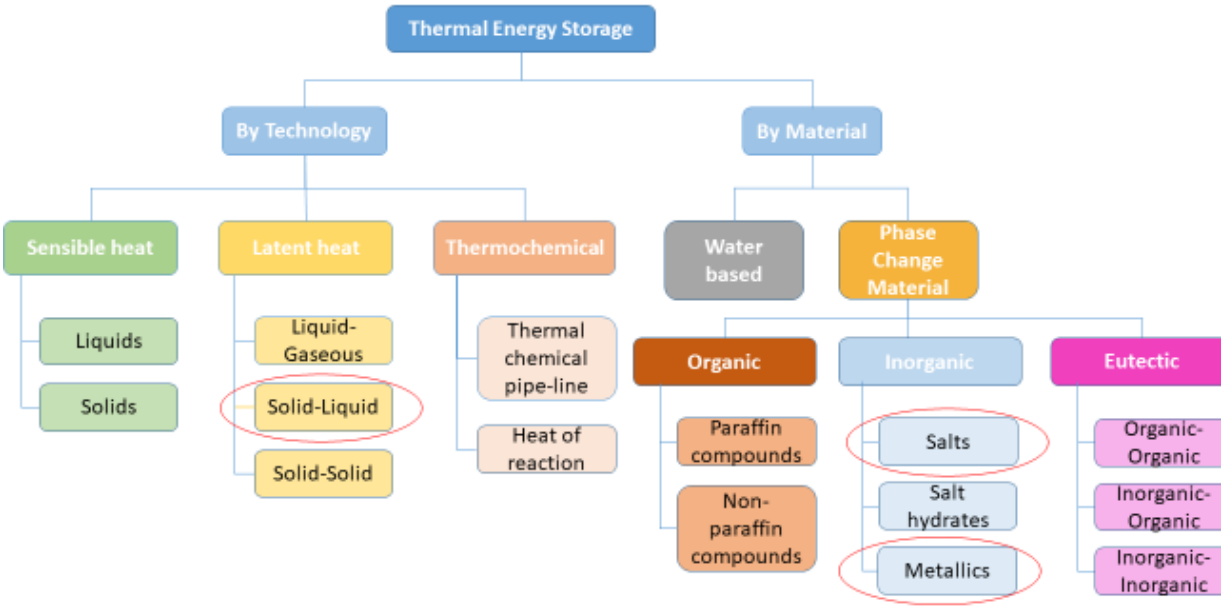

Figure 1: Classification of thermal energy storage systems (in red circles, the main features of storage technologies investigated in this study) [14, 16] .

Among the advantages of those systems are the increase in overall efficiency and better reliability when applied in an energy framework, resulting in better economics, reductions in investment and operating costs, as well as reductions in greenhouse gas emissions [13]. They are flexible decentralized solutions where large-scale heat transfer systems such as district heating and cooling are not practical or are too expensive to apply. However, most current systems are water-based, and their storage capacity is limited by the fact that water storage capacity depends on the operating temperature difference of the heating system used.

Although sensible heat storage is the most common method of thermal energy storage, latent heat storage systems that use Phase Change Materials (PCMs) offer a considerably higher energy density compared to water-based sensible heat storage systems and have the advantage of the isothermal nature of the storage process i.e storing heat compactly in a narrow temperature range [15, 17]. The effect of using PCMs in solar thermal storage systems has been investigated extensively both in experimental and numerical studies [18-24]. Low temperature thermal storage systems (LT-TES) have been sufficiently developed and are currently being used on a commercial level. Companies such as Sunamp ltd, PCM products ltd etc. have commercialized such applications of PCM based TES systems in the domestic or industrial scale, but the focus is only given in low temperature systems.

Recent studies have been directed towards a solution using ultra-high temperature thermal energy storage (UHT-TES) systems, with the utilization of metallic PCMs. These PCMs have the advantage of presenting a high melting point (>1000 ^{o}C), high thermal conductivity and latent heat of fusion which can potentially lead to greater energy densities than the ones achieved in low temperature systems [25, 26]. It is a newly developed concept under on-going research which has been studied in previous work through experimental and theoretical studies including both steady-state and dynamic numerical simulations [26-31]. So far, studies have been focused on the proof of concept, optimization of characteristics (geometry, material etc.), and integration of such a system with a hybrid thermionic photovoltaic (TIPV) electronic converter for parallel conversion of energy to heat and electricity. However, the use of such systems on a domestic level has not been studied to a large extent. Datas et al. has performed a techno-economic analysis on the application of such a system in the residential sector for trigeneration within a solar PV power-to-heat-to-power scheme which also involves other heating systems and latent heat storage technologies apart from this [32].

Our recent study was focused on the thermal performance of a PV- powered UHT-TES system combined with a TIPV converter and its integration with a residential building within a 24 hour period [31]. The scope of this paper is to further investigate the application of such a system in the residential sector and to compare its performance with similar schemes. Several configurations of heating and powering schemes of a typical South European residence are investigated, which include either a LT-TES system or an UHT-TES system coupled with a TIPV converter and they are compared to a reference case of conventional heating which includes only an air-to-water heat pump. A PV system is used in all cases to provide, whenever available, the energy to be used or stored for covering the energy needs for heating and electricity.

2 Methodology

2.1 Description of the examined systems

The implementation of a power-to-heat system scheme with heat storage capabilities in the building sector could be crucial for rational use of renewable energy since it would allow the utilization of the excess electricity generated by renewable energy sources which would otherwise be wasted. In particular, a power-to-heat scheme which includes only a heat pump for example, although efficient due to the high coefficient of performance (COP) of this type of system, allows for a limited percentage of RES exploitation for heat, since it can only exploits RES production only at periods which match the heat demand. A TES system would extend this period, allowing for covering heat demand at other times, when heat demand and RES production do not normally match.

In this analysis, two cases of TES systems are considered, a low temperature TES (LT-TES) used for covering only residential heating needs and an ultra-high temperature thermal energy storage (UHT-TES) system integrated on a building level in order to cover both the electric and heat demand. Those two cases are compared against a reference case which includes an individual heat pump (HP) for covering residential heating requirements. A PV of maximum capacity 15 kW is a common element which is used to power all the cases, the HP in the reference case as well as the studied cases with the TES systems. All these types of heating systems are studied in conjunction with a building and its thermal and electrical needs.

The utilized data of the study involve typical heat and electric demand profiles for a typical South European residence and the electricity production from a PV system which covers the corresponding energy needs when available. The residence location was selected to be in South Europe, since the solar power potential there can be significant for covering a substantial part of the thermal energy needs. A similar methodology with our recent work [33] has also been followed here for specifying the annual heat demand, based on the method of heating degree-hours, which result from the difference ΔT of the hourly environmental temperature, subtracted from a base temperature. Furthermore, the same potential PV production profile and annual electricity demand which has been used in previous work [33] is also considered here. These parameters are presented in graphs which are given in the Annex (Figure 17, Figure 18, Figure 19 and Figure 20 respectively).

2.1.1 Reference case

The reference case (Figure 2) includes a heat pump (HP) for covering the residential heating requirements. The HP uses the R134a as a refrigerant medium and includes an electric motor driven compressor, which is powered by a PV of 15 kW_p capacity.

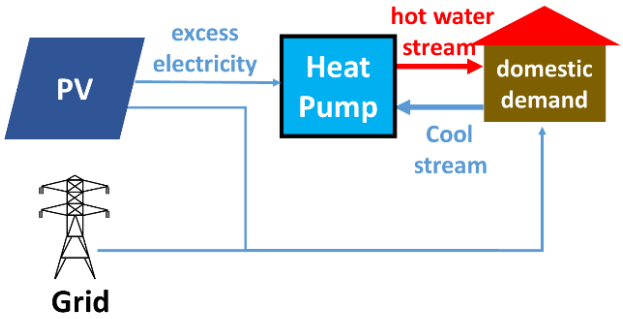

Figure 2: Schematic diagram of a PV-powered heat pump connected to residential heating

2.1.2 Low Temperature TES (LT-TES)

The Low Temperature TES (LT-TES) system consists of a closed container, which contains an inorganic, Sodium Acetate based PCM which stores thermal energy as it changes phase from solid to liquid. Within the PCM, a tube coil is immersed, which transfers the heat stored from the PCM to the heating medium, usually water, for covering the residential heat demand. Thus, this storage system, also known as a heat battery, is practically a heat exchanger with a container filled with PCM. A variety of heat sources can be used to charge the heat battery, including, electricity from the grid or from a PV, heat from a heat pump, hot water from a boiler or district heating.

Two subcases of LT-TES are investigated in this study, which are distinguished by the heat source used for charging the heat battery: a) heat supplied from an internal electric resistor, powered by the PV system. (Figure 3a) and b) heat supplied from hot water by a heat pump which flows in the heat battery through an internal tube coil (Figure 3b).

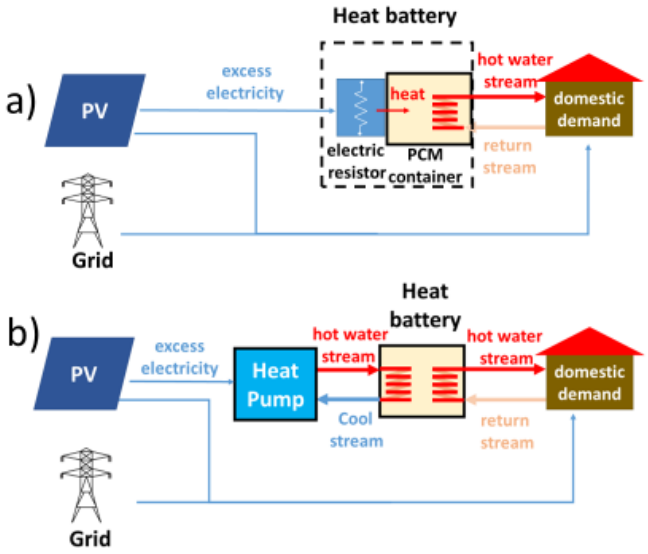

Figure 3: Residential thermal consumption covered by Heat Battery using a) electric resistor as a heat source b) hot water from a heat pump as a heat source

2.1.3 Ultra-High Temperature TES (UHT-TES)

The investigated UHT-TES/TIPV system (Figure 4) consists of a series of interconnected components; a silicon-based UHT-TES module, a heat-to-electricity solid-state device and a copper plate heat spreader. The heat-to-electricity device, i.e. a hybrid thermionic-photovoltaic (TIPV) converter, consists of two electrodes -a hot emitter and cold collector- separated by an ultra-high vacuum gap. During operation, the TIPV emitter is heated up directly by the PCM container, reaches ultra-high temperatures (>1000 °C) and starts emitting photons and electrons towards the TIPV collector. By this manner, high temperature thermal energy is directly converted into electricity. At the TIPV collector rear side, where the PV cell resides, the copper plate heat spreader acts as a heat sink of the excess thermal energy [30, 34]. In this type of cooling system, water is used as a cooling medium. The whole system can operate in two modes, separately or at the same time, charging and/or discharging. In charging mode (daytime), the PCM vessel stores thermal energy produced from an electric resistor in the form of latent heat. During discharging period, the TIPV device connected to the UHT-TES system converts part of the stored thermal energy into electricity and any remainder is utilized as high enthalpy thermal energy, through effective heat recovery.

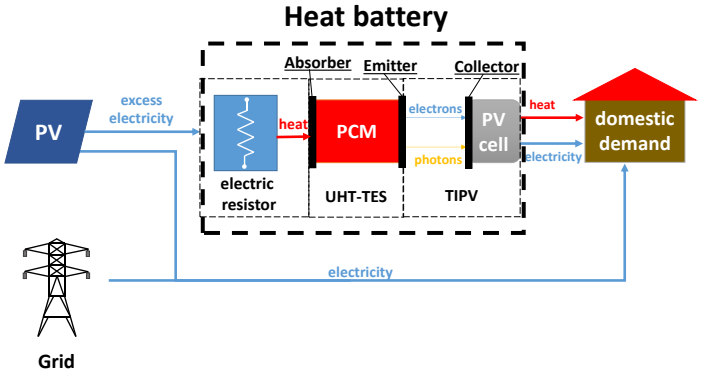

Figure 4: Flow chart of the UHT-TES/TIPV system.

The heat storage block is charged when there is available power coming from the PV system and discharged when there is a corresponding heat and/or electricity demand. In this assessment, two different strategies for discharging are investigated, i.e. a) covering heat demand as a priority or b) covering electricity demand as a priority. In the first one, the heat load is served as a priority, which means that at every moment the power output from the heat storage system is set in that way so that the share which corresponds to the produced heat can cover as much share from the heat demand as possible. The remaining extracted energy is converted to electricity at a specified ratio, with the target to cover as much of the electric demand as possible. In the second case, the electricity demand is served as a priority. Similarly, the power output from the heat storage system is set in that way so that the share which corresponds to the produced electricity can cover as much share from the electricity demand as possible and the remaining is converted to heat at the specified ratio.

2.2 Model description

The cases under examination are summarized in Table 1. For each of the cases which include heat storage (Cases 1 and 2), three different heat battery capacities have been considered: 3 kWh, 10 kWh and 40 kWh.

A model has been developed for each of the cases to calculate the heat covered and the electricity required in each case. All the models have been developed in Dymola, a tool for dynamic multi-domain modeling and simulation which uses the open-source Modelica programming language. In particular, components have been taken from the default Modelica Library, or other existing libraries when available or they have been developed from scratch when necessary. More information about the model compounds are given below.

Table 1. Examined cases description

# Case	PV	Heat source	TES type	Comment
Reference	yes	hot water from a heat pump	no TES	
Case 1a	yes	electric resistance	LT-TES	
Case 1b	yes	hot water from a heat pump	LT-TES	
Case 2a	yes	electric resistance	UHT-TES	Heat priority strategy: covering heat demand as a priority
Case 2b	yes	electric resistance	UHT-TES	Electricity priority strategy: covering electricity demand as a priority

The calculations for each case have been performed with a time step Δt =1h for a one-year period analysis, which is considered adequate to depict all the changes and the dynamic behavior within that period.

2.2.1 Reference case (PV+HP)

The reference case includes a heat pump (HP) for covering residential heating requirements. The HP is powered either by a PV of maximum capacity 15 kW or from the grid. Components from the Thermocycle library [35] have been used, which is an open-source Modelica library for dynamic modeling of thermal systems. Besides the standard refrigerant cycle components (compressor,

condenser, expansion valve and evaporator) there are also two PID controllers involved in the operation of the heat pump, which work simultaneously and in parallel to regulate the heat pump capacity. The first one is used for keeping constant the superheating temperature difference of the refrigerant at the exit of the evaporator, by controlling the opening of the valve. The second one keeps constant the output water temperature of the condenser by controlling the frequency of the electric motor which specifies the rotational speed of the compressor and subsequently the refrigerant mass flow. The model also includes some auxiliary components, namely sensors and input and output stream components. The layout of the model with all the components included is presented in Figure 5.

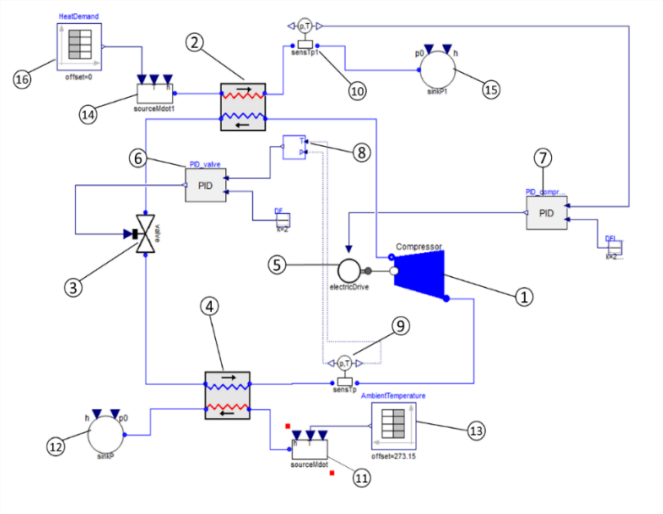

1) **Compressor**
2) **Condenser**
3) **Valve**
4) **Evaporator**
5) **Electric motor**
6) **PID for controlling the valve**
7) **PID for controlling the compressor**
8) **Block for calculating ΔT from saturation point**
9) **Temperature and pressure sensor**
10) **Temperature sensor**
11) **Input air mass flow source component**
12) **Air pressure sink component**
13) **Ambient air temperature time table**
14) **Water temperature source component**
15) **Water pressure sink component**
16) **Input water mass flow time table**

Figure 5: Layout diagram of heat pump model

After modeling the heat pump, a chart of the COP of the heat pump was derived, based on the input ambient air temperature and the heat output of the heat pump (Figure 6a). Based on this chart, a simple model has been developed, intended to replace the previous one, which uses just a table component, for faster calculation of the COP and the electricity consumption of the heat pump (Figure 6b). This table component uses two inputs, the ambient air temperature and the targeted heat production based on the heat demand t and the output is the COP. Based on the COP and the heat demand, the total electricity consumption can be defined and based on the PV production (Figure 19), the percentage of energy which is covered by the PV can be calculated.

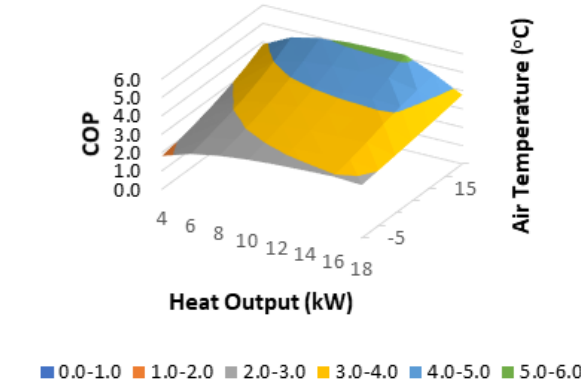

a)

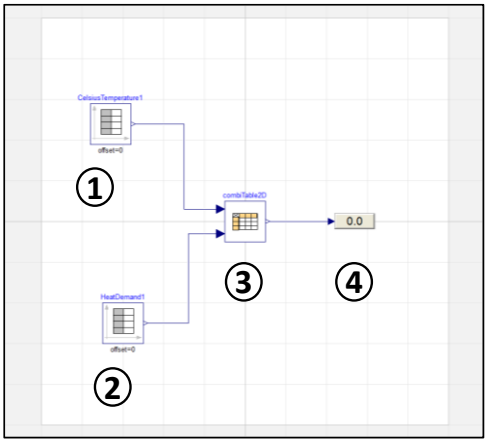

1) Ambient Temperature input table
2) Heat Demand input table
3) COP chart table
4) COP output value

b)

Figure 6: a) Chart of COP based on air temperature and heat output of the heat pump and b) Simplified heat pump model based on COP chart

2.2.2 Case 1 (LT-TES)

2.2.2.1 Case 1a: LT-TES with electric resistor

In this case, the heat battery model includes a resistor with variable electric resistance, whose value is set according to the power output of the PV system. The model includes seven basic components (Figure 7a): a time table which has registered data for the PV power production (1), a charge control (2), a heat storage (3), a discharge control (4), a constant voltage which simulates the output voltage of the PV system (5), a ground component (6) and a time table which has registered data for the heat demand (7).

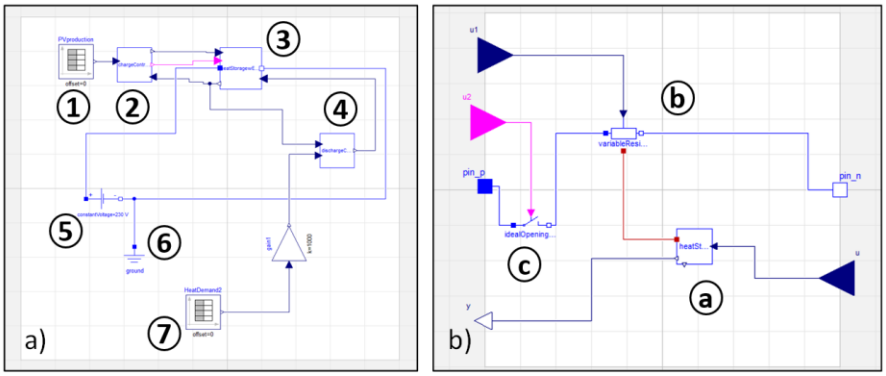

1) **PV production input table,**
2) **Charge Control Unit,**
3) **Heat storage component,**
4) **Discharge Control Unit,**
5) **Constant Voltage component,**
6) **Ground component**
7) **Heat Demand input table**

a) **Energy balance solver**
b) **Variable Resistor**
c) **Switch**

Figure 7: a) Model of heat battery with a variable electric resistance as a heat source b) Heat storage component

The heat storage component (4) consists of the following particular subcomponents: a component which solves the energy balance equation of the heat battery (a), a variable resistor (b) and a switch (c) which controls the electricity flow through the resistor. The subcomponents of this model are presented in Figure 7b.

The heat storage component also includes some connectors which facilitate the data flow between the components, such as the input of the heat demand data (u), the variable resistance value (u1), a Boolean signal which controls the switch (u2) and the output of the value of state of charge (SOC) of the battery (y), as well as positive and negative pins (pin_p and pin_n) for connecting the switch and variable resistor to an electric circuit, as shown in Figure 7b.

The following equation is solved in the energy balance equation solver component:

$$\frac{\mathrm{d}E}{\mathrm{dt}} = P - Q \qquad (1)$$

where *E* is the stored energy in the heat battery, *P* is the input power from the electric resistance and *Q* is the heat demand served. The state of charge (SOC) of the heat battery is also defined in this component as follows:

$$SOC = \frac{E}{E_{max}} \qquad (2)$$

where E_{max} is the maximum capacity of the heat battery as specified by the manufacturer. The maximum capacity of the heat battery is defined to be 3, 10 or 40 kWh, depending on the case examined.

The energy balance component which is fed with the proper values of *P* from the variable resistor (b) and *Q* from the Heat Demand input table (7) through the discharge control (6), solves the equation and determines the energy *E* stored in the battery, and subsequently, the state of charge (SOC) of the battery.

The variable value of resistance is dictated by the charge control component which is responsible for controlling the input of heat in the heat battery. The resistance of the resistor is calculated according to the equation:

$$R = \frac{V^2}{P} \quad (3)$$

where *R* is the electric resistance of the resistor, *V* is the voltage applied to the resistor, set to a constant value of 230 V and *P* is the electric power produced by the PV, which is converted to heat in the electric resistor.

The charge control unit also determines when the circuit is switched on and off. It is switched off when the battery is fully charged but also when there is no electric power produced by the PV and switched on at any other time, i.e. when there is available electric power produced and the heat battery is not fully charged at the same time. This determines how much of the available PV power will be used by the battery and defines the proper value of P in equation (1). The discharge control component controls the input of heat demand *Q* to the heat storage component and energy balance solver subcomponent. This value Q reflects the amount of heat demand that can be served by the heat battery in each hour. The discharge control simply sets the input value equal to zero when the heat battery is fully discharged and cannot serve the demand, and equal to the value of the domestic heat demand at any other time. The domestic heat demand is imported from a timetable component (7) which has the data from Figure 17 registered.

2.2.2.2 Case 1b: LT-TES with heat pump

This configuration (Figure 8) includes the same components for solving the energy equation of the heat battery (5) as in the previous case, but also an extra component modeling the heat exchanger (4) which provides the heat to the PCM. Besides those, a heat pump which is represented by the simplified heat pump model mentioned in the reference case (Figure 6b) is included. Therefore, the COP chart table component (2) and the Ambient Temperature input table (1) from that case are part of this model, too. Other components used in this model include a charge control component (7), which controls the heat pump on-off operation according to the charging strategy selected, a time table which has registered data for the PV power production (3) and the heat demand (6), as well as a group of components (8) with mathematical and logical functions used for unit conversion, water mass calculation, as well as other monitoring and control checks (threshold component, division component, logical switch for conditional comparison, monitoring components)

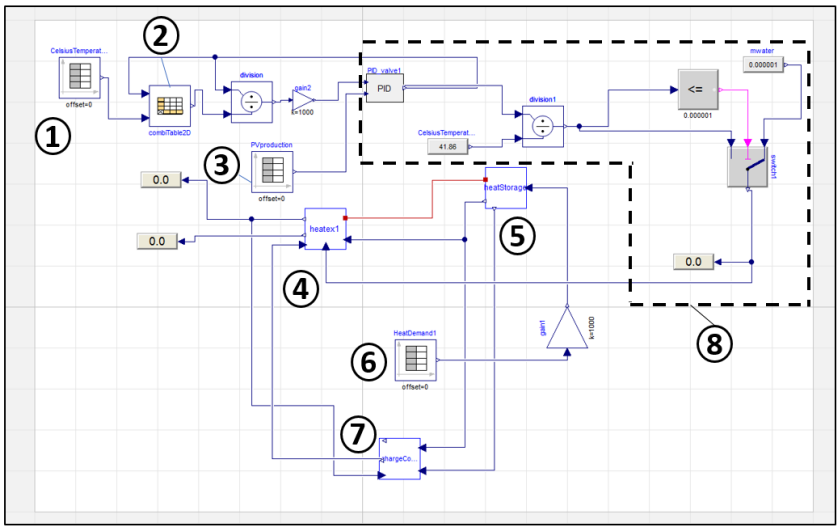

1) Ambient Temperature input table,
2) COP chart table,
3) PV production input table,
4) Heat exchanger component,
5) Energy balance solver,
6) Heat Demand input table,
7) Charge Control Unit,
8) Unit conversion and calculation components

Figure 8: Model of heat battery heated by heat pump through internal heat exchanger (Type 2)

The energy balance solver component (5) is the same as the one described previously and solves the same equations (1) and (2). The maximum capacity of the heat battery E_{max} in equation (2) is again considered to be 3, 10 or 40 kWh depending on the case. The same time table component with the domestic heat demand data from Figure 17 is also included here. The data from this time table (6) are used as an input to the energy balance solver component and define the value of Q in equation (1). The heat exchanger (4) calculates the heat transferred to the PCM from hot water which is heated by the heat pump, and defines the value of P in equation (1). The heat exchanger component follows the method as presented in [17]. The tube of the heat exchanger is considered to be spatially discretized into n parts or n+1 nodes. In this case n=100.

The equations which are solved for each node i are the following:

$$\dot{Q}_{HEX,i} = \dot{m}_{HTF} \cdot c_{p,HTF} \cdot \left(T_{HTF,i+1} - T_{HTF,i}\right) \tag{4}$$

$$\dot{Q}_{HEX,i} = A \cdot U_{HTF,i} \cdot \Delta T_{ln,i} \tag{5}$$

$$\Delta T_{\ ln,i} = \frac{T_{pc} - T_{HTF,i+1} - \left(T - T_{HTF,i}\right)}{\ln \frac{T_{pc} - T_{HTF,i+1}}{T_{pc} - T_{HTF,i}}} \tag{6}$$

$$U_{HTF,i} = \frac{1}{\frac{1}{a_{HTF,i}} + \frac{r_{in}}{\lambda_{Tc}} \ln \frac{r_{out}}{r_{in}} + \frac{r_{in}}{\lambda_{eff}} \ln \frac{r_{pcm}}{r_{out}}} \tag{7}$$

$$a_{HTF,i} = \frac{Nu \cdot k_{water}}{2 \cdot r_{in}} \tag{8}$$

$$\lambda_{eff} = \begin{cases} \lambda_{eff,s}\,, if\ SOC = 0 \\ SOC \cdot\ \lambda_{eff,l} + (1 - SOC) \cdot \lambda_{eff,s}\,, if\ 0 < SOC < 1 \\ \lambda_{eff,l}\,, if\ SOC = 1 \end{cases} \quad (9)$$

From the above equations, the total heat transferred to the PCM can be calculated as the sum of the heat flows from each individual part of the tube coil, according to the following equation:

$$\dot{Q}_{tot} = \sum_{i=1}^{n} \dot{Q}_{HEX,i} \quad (10)$$

The input and output temperature of water for each part are also specified. The convective heat transfer coefficient between the heat transfer fluid and the inner tube wall, a_{HTF} , is calculated according to eq. (8) based on the definition of Nusselt number for which an empirical correlation for flow regimes in the transition zone between laminar and turbulence introduced by Gnielinski [36] is applied. The effective thermal conductivity values of the PCM heat exchanger compound for solid and liquid phase correspondingly are taken from [17] and are equal to $\lambda_{eff,s} = 3.25\ W/mK$ and $\lambda_{eff,l} = 8.75\ W/mK$.

Finally, the heat pump is represented by the same simplified COP chart table component used in the reference case. In this case, the heat output is specified retrospectively using a PI controller which varies the heat output of the heat pump in order to set the electricity consumption to match with the known PV production. From this heat output, and assuming that the heat pump operating temperatures of water are 60°C at the inlet and 70°C at the outlet, the mass of the heated water is derived which is then used as an input to the previously described heat exchanger. Those calculations are performed through the components grouped and labelled as (8) in Figure 8.

2.2.3 Case 2 (UHT-TES)

In this case, an innovative energy storage system design that utilizes an ultra-high temperature phase change material is investigated. In this configuration the heat battery is charged through an electric resistor, storing thermal energy in the form of latent heat as in the previous cases, but at ultra-high temperatures. The PCM, which is contained in an insulated crucible, is pure silicon with a melting point of approximately 1400°C. During the discharging period, the stored thermal energy is converted into electricity through a TIPV converter, which also allows for thermal energy production.

A 1D dynamic model (Figure 9), which calculates the temperature profile of the PCM heat storage, as well as the supplied thermal and electric energy has been developed. In this model, the same PV to the previous cases is used for feeding the UHT TES. The model includes a basic PCM heat storage component, a charge control unit and some time tables with all the data which are used as inputs (PV production, heat and electricity demand).

1) PCM storage component,
2) Charge Control Unit,
3) PV production input table,
4) Heat Demand input table,
5) Electricity Demand input table

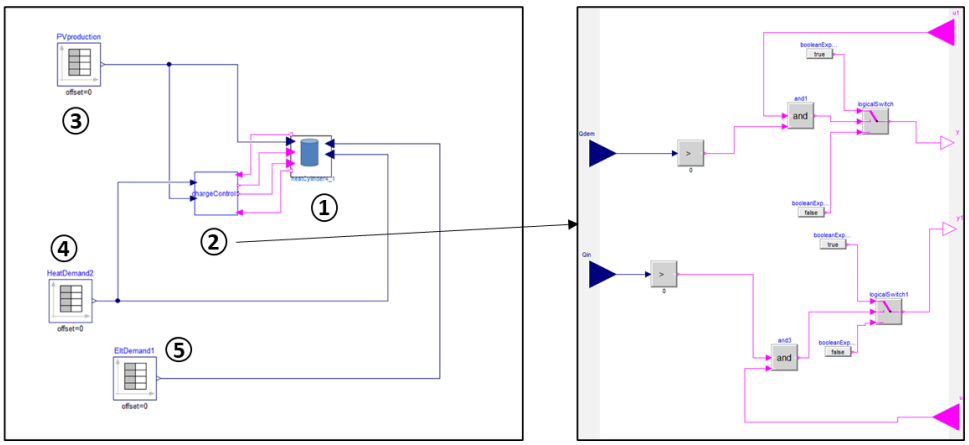

Figure 9: a) 1D model developed for the UHT-TES/TIPV converter and b) Charge Control Unit

The simulated case considers a basic geometry of a cylinder for the heat storage component, as seen in Figure 10, which has been investigated in previous work [37] and has been proven advantageous regarding charging and discharging time compared to other geometries.

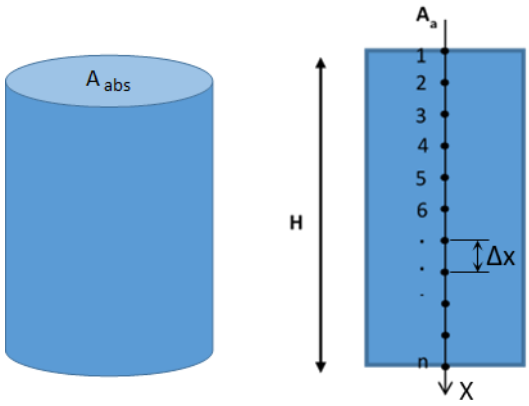

Figure 10: Geometry and discretization display of the Dymola 1D model

The heat storage component is based on the enthalpy-porosity approach to simulate the PCM solidification/melting process, an implicit method to track the solid-liquid phase change front, originally proposed by Voller et al. [33]. The heat flux imposed at the emitter surface during discharge is calculated according to the following equation:

$$Q_e = -(3.17E-04 * T_{em}^3 - 0.7616 * T_{em}^2 + 6.438E02 * T_{em} - 1.8385E05), \quad (11)$$

where T_{em} is the emitter temperature. The temperature at each point is calculated based on the energy balance equation:

$$\frac{\partial[\rho c_p \cdot (T - T_{ref})]}{\partial t} + \Phi = \frac{\partial\left(k \cdot \frac{\partial T}{\partial x}\right)}{\partial x} - Q_{loss} \quad (12)$$

where T is the temperature at a point of the PCM, T_{ref}, the reference temperature (25ºC or 298.15 K) ρ, the PCM density (kg·m^{-3}), c_p the specific heat capacity (J·kg^{-1}·K^{-1}) and k the thermal conductivity of the PCM (W·m^{-1}·K^{-1}).

For the estimation of useful heat and electricity production it is assumed that the stored thermal energy in the form of latent heat in the LHTES module is converted into both electricity and heat at a 32%-68% ratio, according to the electrical conversion efficiency of the TIPV unit [38]. The heat output is totally collected by the coolant and utilized to cover any heat demands. Heat losses from the crucible walls in this case are neglected. More details about the model can be found in previous study [37].
For the discretization, the number of nodes used were n=402 and the time step was Δt=1h. Different values have been considered for the PCM properties at its solid and liquid phases.
As mentioned earlier, three different heat battery capacities have been considered (3 kWh, 10 kWh and 40 kWh), which correspond to different geometric dimensions. The ratio of cylinder height to diameter (H/D) was kept constant in all cases. The material properties used for modeling the examined cases are presented in Table 2 below and the geometric characteristics in Table 3.

Table 2: Material properties of PCM

Parameter	Symbol	Value
Thermal conductivity	k_s	20 $W \cdot m^{-1}K^{-1}$
	k_l	60 $W \cdot m^{-1}K^{-1}$
Specific heat	c_p	1040 $J \cdot kg^{-1}K^{-1}$
Density	ρ_s	2330 $kg \cdot m^{-3}$
	ρ_l	2570 $kg \cdot m^{-3}$
Melting point	T_l	1681 K
Solidification point	T_s	1679 K
Latent heat of fusion	L	$1.8 \cdot 10^6$ $J \cdot kg^{-1}$

Table 3: Geometric characteristics of heat storage

Heat storage capacity		3 kWh	10 kWh	40 kWh
Height	H	0.1122 m	0.1677 m	0.2661 m
Absorber surface	A_{abs}	0.0230 m^2	0.0512 m^2	0.1291 m^2

The charging and discharging strategy is applied by a separate component as seen in Figure 9b, which simulates a charge control unit. This unit outputs specific signals that control when the heat storage system enters or leaves a charging and/or discharging state. When the heat storage system is neither at a charging nor at a discharging state, the heat storage component is basically in a stand-by mode, in which the heat is neither absorbed nor emitted and just stored in the form of latent heat. The heat storage block is charged when there is available power coming from the PV system and discharged when there is a corresponding heat and/or electricity demand and there is available energy stored in the heat battery.

3 Results and Discussion

3.1 Dynamic behavior analysis on weekly period

A profile of the dynamic behavior of the heat battery during winter time on a weekly period (2nd week of January) is presented for each case (i.e. reference case in Figure 11, Case 1a and 1b in Figure 12 and

Cases 2a and 2b in Figure 13). The supply of heat from the heat pump (reference case) or from the heat battery in the other cases (stored heat supply) and the domestic heat demand as well as the electricity production, where applicable (Cases 2a and 2b) and the domestic electricity demand are presented for the investigated cases with a heat battery capacity of 40 kWh. The electricity from the PV absorbed by each heat storage system is also presented for each system along with the PV potential production. The total energy stored in the heat batteries is also presented for Case 1a and 1b.

Seven clear cycles can be distinguished in most cases corresponding to the electricity input from the PV at each day of the week. Some exceptions are in the heat and electric supply of Case 2a and 2b where less than seven distinct cycles of discharging can be seen because in these cases either there was no demand or the conditions for discharging have not been fully satisfied according to the charging control strategy. Furthermore, less than seven cycles can also be observed in the stored energy of Case 1a and 1b, because in some of the days the energy provided by the PV as input is directly supplied to the demand as a total, not leaving a remaining amount of energy to be stored.

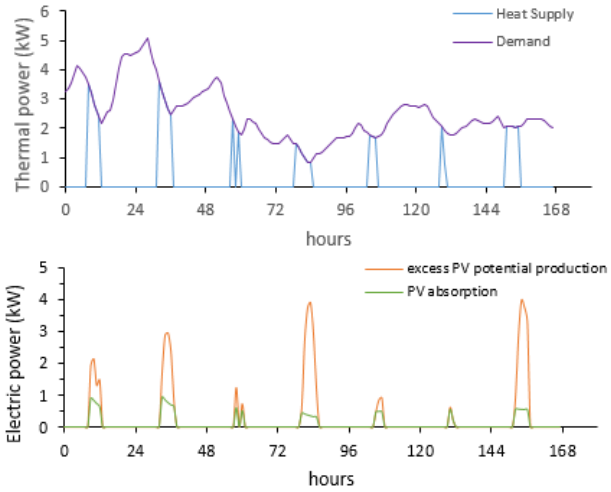

Figure 11: Dynamic behavior of heating system (Reference case) on a weekly period

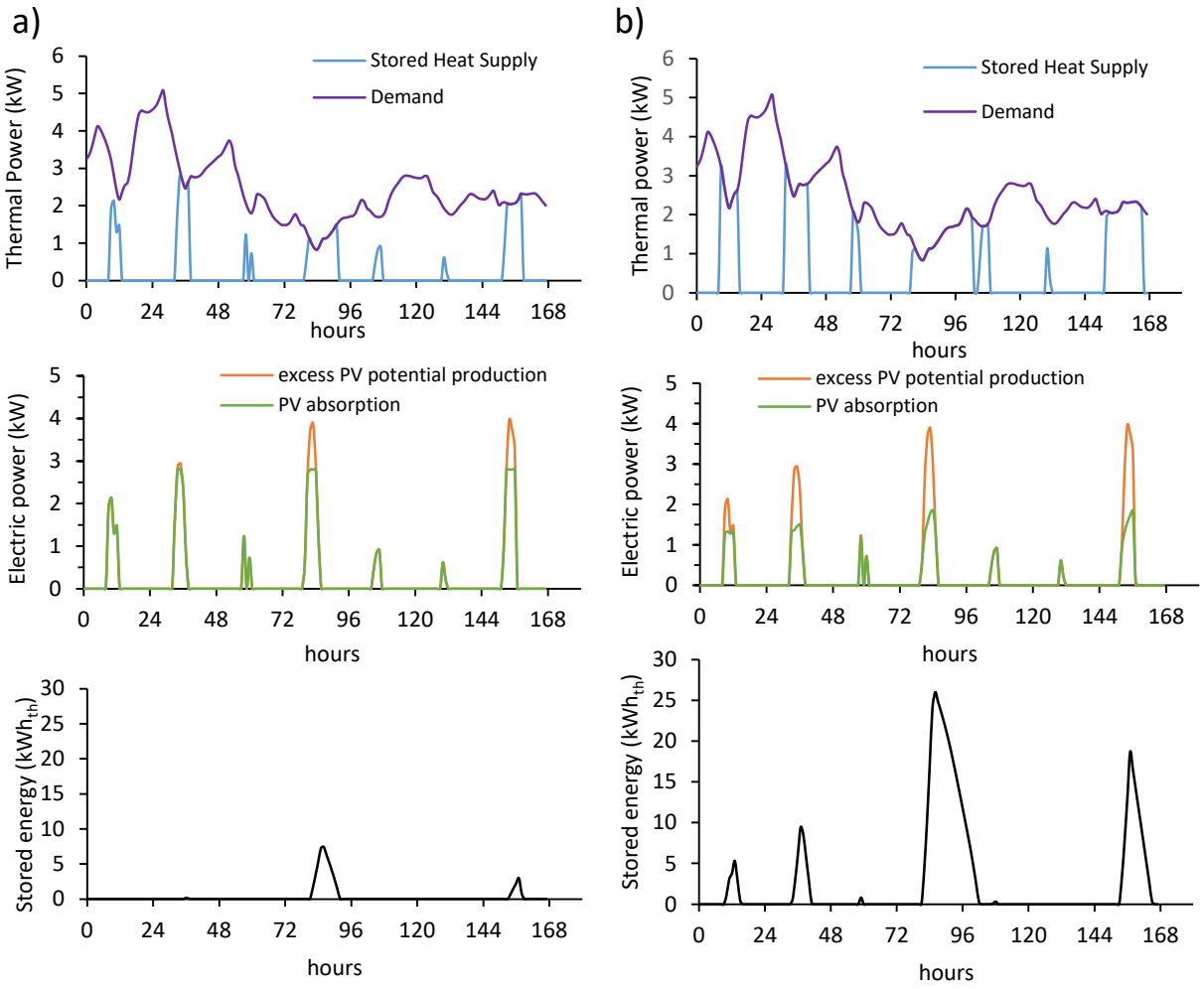

Figure 12: Dynamic behavior of heat storage system for a) Case 1a and b) Case 1b on a weekly period

As seen in Figure 11, a considerable amount of the produced PV electricity at the reference case is not used to cover the electricity demand of the house and if no absorption from the grid is foreseen, it is lost (curtailed). This happens during midday of the sunny days, where the total electrical demand is relatively low. It is observed that PV absorption is higher in any other case with a heat storage scheme. Especially in Cases 2a and 2b the PV potential production is fully absorbed (Figure 13).

Something notable is that Case 1a presents better PV absorption than Case 1b (Figure 12), as it includes an electric resistance for converting electricity to thermal power, while Case 1b includes a heat pump for this purpose. Electric resistance has a COP=1, in contrast to the heat pump, which has COP>1. This means that more electricity is required by the resistance in Case 1a than the heat pump in Case 1b to get the same amount of heat. On the other hand, Case 1b presents more coverage of heat demand than Case 1a, despite the fact that less electricity is used. This is also because of the fact that a heat pump has COP≈3, which means that with less electricity, more heat is produced and consequently stored in the heat battery.

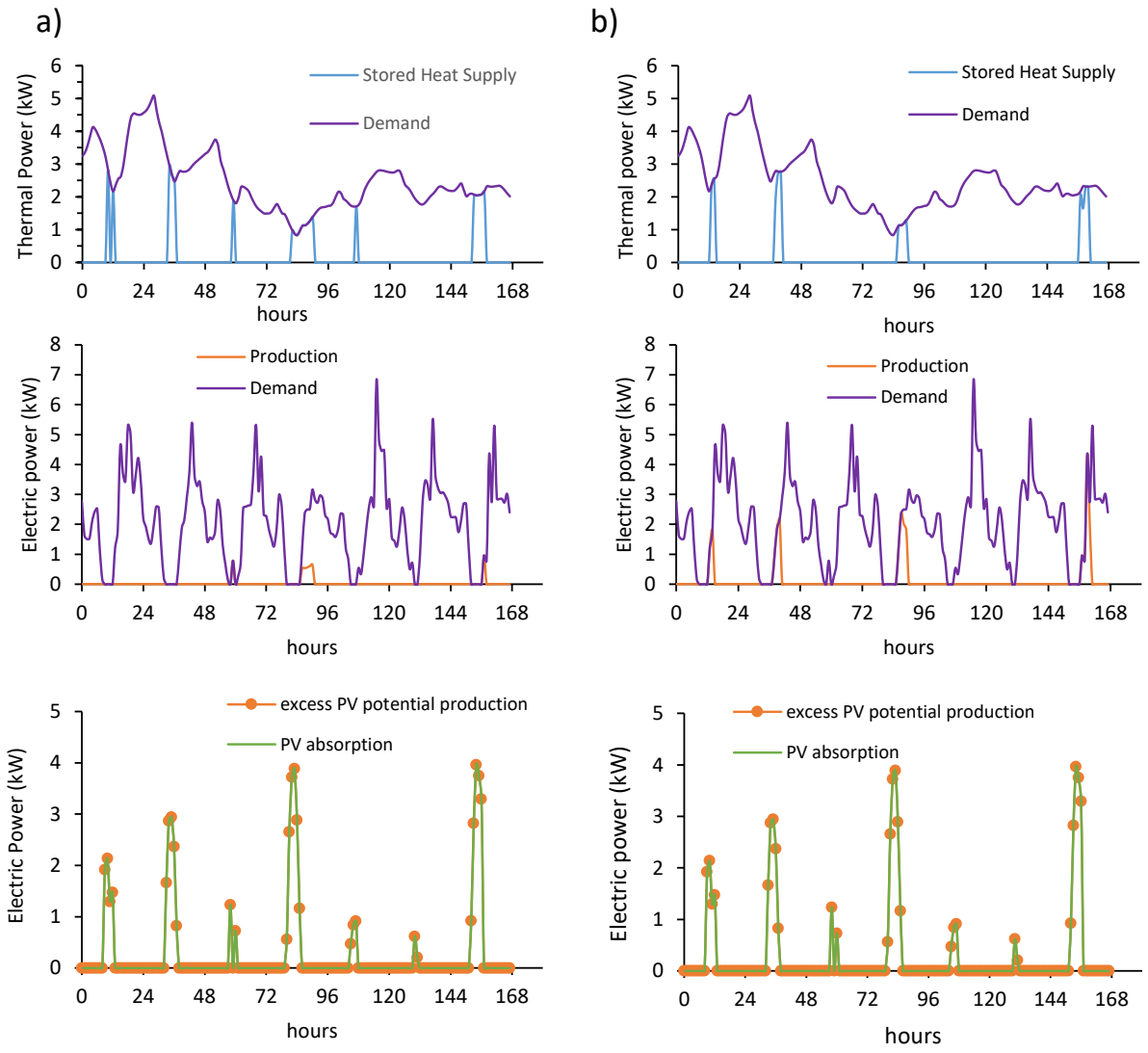

Figure 13: Dynamic behavior of heat storage system for a) Case 2a and b) Case 2b on a weekly period

Another noteworthy point is that coverage of heat and electricity demand for Cases 2a and 2b is relatively low (Figure 13), despite the fact that utilization of produced electricity is quite high, reaching full PV absorption. The high PV absorption is explained again due to the fact that an electric resistance with COP=1 is also used as a means to convert electricity to heat, therefore a lot of electricity is required to produce adequate heat. The low coverage of heat and electricity demand is partially due to the limitations imposed through the charging control unit and partially due to the limited PV production in winter time. Besides, none of the examined cases covers fully the heat or electricity demand in the investigated period for the same reason.

For Cases 2a and 2b it can also be observed that with the current discharge strategy, electricity demand is covered as soon as there is available stored energy in the heat battery. Focusing on the use of heat batteries as a method to achieve peak shaving of the electricity demand, a modified discharge strategy could be applied for those cases, that would take into account the peaks of the electricity demand and would supply electricity specifically during those periods. Thus, peak shaving could be achieved in a

smaller residential scale. However, if this effect is reproduced in multiple residencies, it could also have an essential contribution in peak shaving of the total electric demand, relieving the grid from high demand during power “rush hours”.

3.2 Energy flow analysis and Effect of Heat Battery size

The resulting heat and electricity supply per hour for covering the corresponding demand have been calculated, and the percentage of heat and electricity demand covered from RES in each case is presented in Figure 14 and Figure 15 on a monthly basis. The PV usage on a monthly basis, i.e. the percentage of available PV power actually used for covering heating and electrical demand is shown in Figure 16. Table 4 finally shows the same parameters but on an annual basis and other basic energy-flow related annual parameters.

It is clearly shown that the case with the LT-TES which also includes a heat pump (Case 1b) covers the most heat demand as a total for the whole year (Table 4), and for each month individually for all the capacities of the heat battery (Figure 14). Case 1a with the electric resistance exceeds the total heat demand coverage of the reference case only for battery capacities of 10 kWh and 40 kWh. On a monthly basis, it manages to cover more heat demand than the reference case on March, April and December for the capacity of 3 kWh, and all months except for November for battery capacities of 10 kWh and 40 kWh. At all circumstances, Case 1b covers more heat demand than Case 1a.

Cases 2a and 2b with the UHT-TES both cover less heat demand than the LT-TES cases as a total (Table 4), but Case 2a covers more heat demand than 2b in all circumstances (Figure 14 and Table 4), which is expected, as it is the UHT-TES case optimized for heat output. Case 2a also covers more heat demand as a total than the reference case for heat battery capacities of 10 kWh and 40 kWh (Table 4). On a monthly basis (Figure 14), Case 2a only manages to exceed the reference in April for the 3 kWh capacity, March and April for the 10 kWh capacity and from January to April for the 40 kWh capacity, exceeding even Case 1a in March. Case 2b seems to be the case with the least heat coverage, exceeding the reference case only in April for the 40 kWh capacity.

Regarding the electricity coverage, Cases 1a and 1b have no difference from the reference case (Figure 15 and Table 4), since unlike Cases 2a and 2b, none of the heat batteries used provides electricity and therefore the electricity coverage depicted in the graph corresponds only to the energy supply covering domestic needs directly from the PV. Between the two cases which do also supply electricity, Case 2b which corresponds to the electricity priority strategy provides the most electricity coverage in all circumstances. It can also be concluded that the larger the battery capacity, the higher the electricity coverage is.

A comparison between the exploitation percentage of the produced energy from PV in each of the cases is also given below. Regarding the PV usage, all the examined cases present a better performance than the reference. In particular, Cases 2a and 2b are distinguished for the highest PV usage, with Case 2b being more prominent and Case 1a closely following Case 2a. On a monthly basis (Figure 16), there are months in which Case 2a and Case 1a sometimes reach or even exceed the PV utilization of Case 2b, but as a total (Table 4), Case 2b exceeds all other cases.

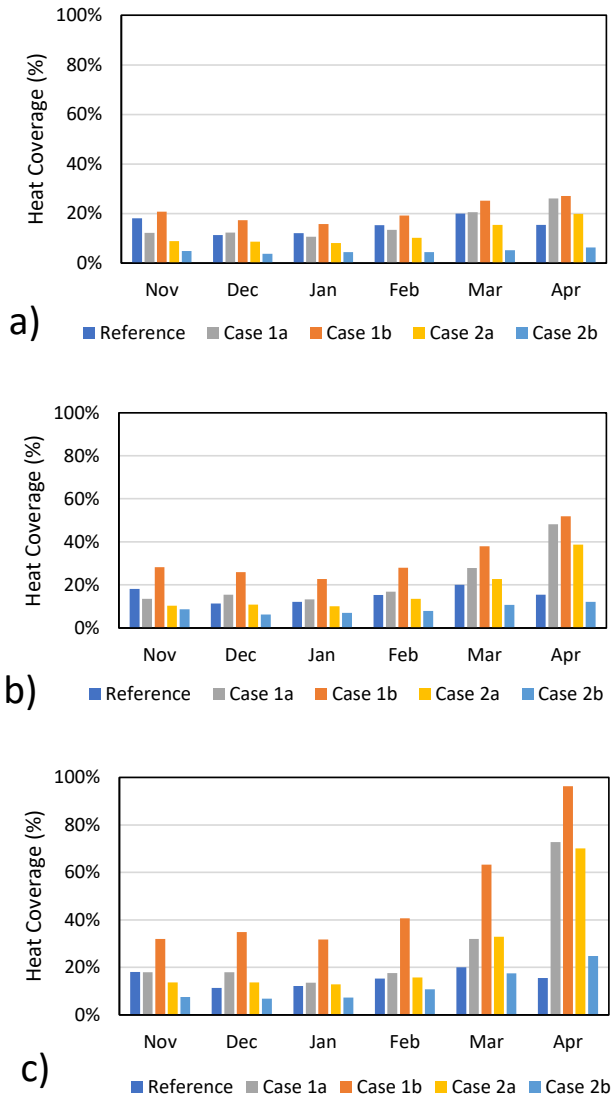

Figure 14: Comparison of heat coverage during the heating period (Dec-Apr) using Heat Battery with capacity a) 3 kWh, b) 10 kWh and c) 40 kWh

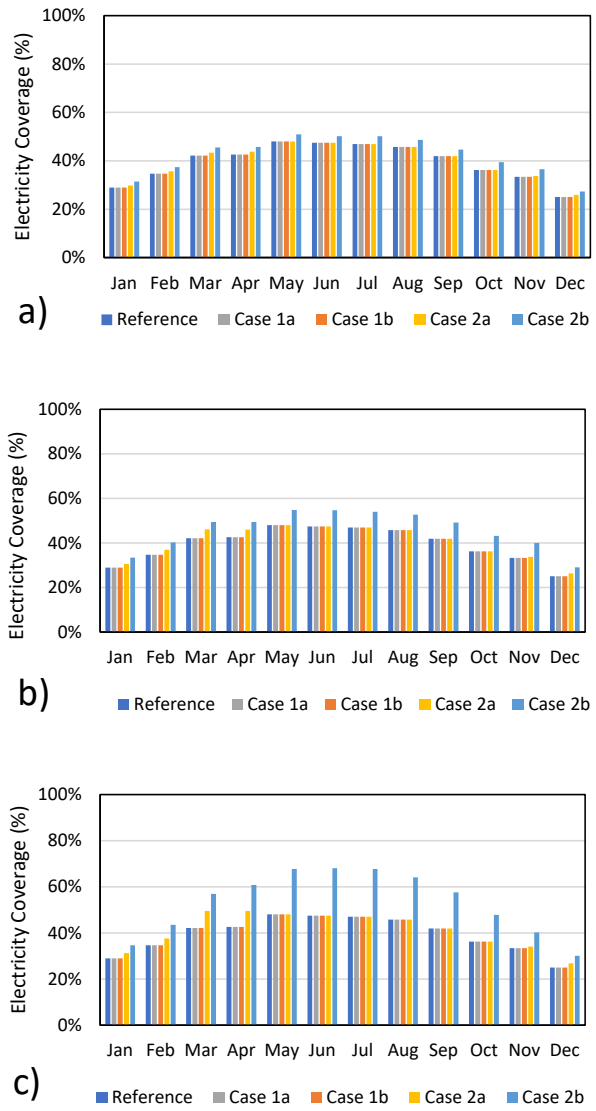

Figure 15: Comparison of electricity demand coverage per month using Heat Battery with capacity a) 3 kWh, b) 10 kWh and c) 40 kWh

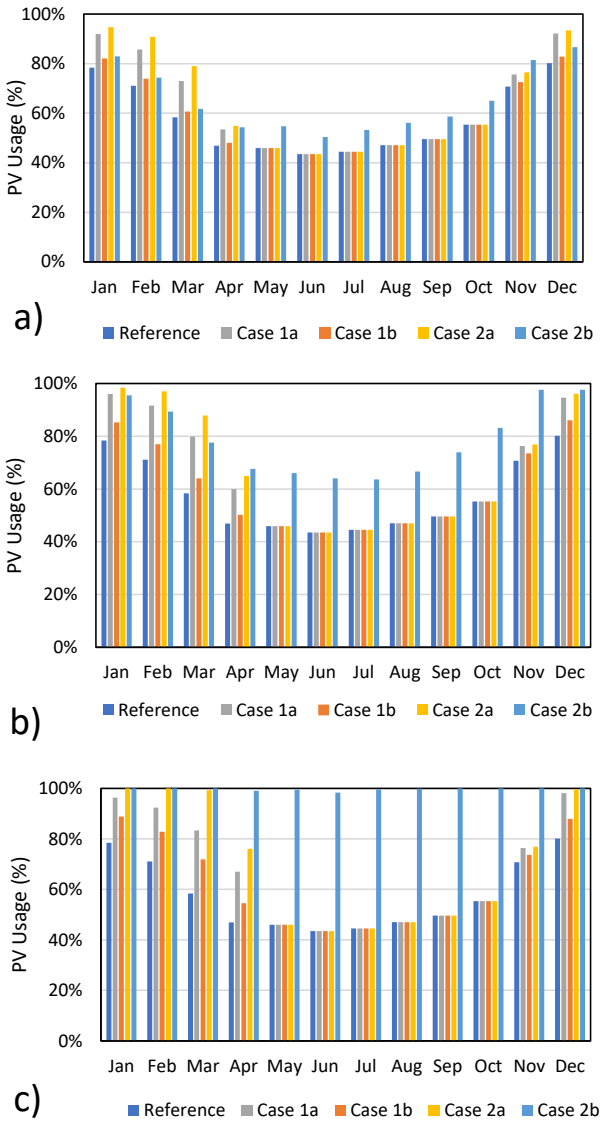

Figure 16: Percentage of available PV power absorbed per month using Heat Battery with capacity a) 3 kWh, b) 10 kWh and c) 40 kWh

Table 4 presents basic energy-flow related parameters on an annual basis, such as the aforementioned annual heat and electric coverage percentage, PV usage percentage, but also the annual PV energy absorption (in kWh) as well as the needs for grid electricity and additional heat consumption from non-RES (also in kWh). There is a clear increasing trend of heat coverage, PV usage percentage and PV absorption according to the increase of heat storage capacity. Moreover, especially for Case 2, an increase in utilization of electricity derived from the PV with the increase of storage capacity is also observed. As a consequence, the annual consumption of electricity from the grid is decreasing, which leads to electricity cost reduction. Those savings correspond to a decrease in electricity consumption from the grid compared to the reference case, ranging between 0.7% with a 3kWh battery capacity,

1.75% with a 10 kWh capacity and 3.0 % with a 40 kWh capacity for Case 2a and between 4.8%, 10.55% and 22.7% respectively for Case 2b.

For full heat coverage, additional heating from an energy source other than the available PV would be required since none of the cases can fully cover heat demand. The reference case and Case 1b which include a heat pump could use it with power from the grid for covering the extra heat demand required. On the other hand, Case 1a, 2a and 2b would require an extra heating system to serve the remaining heat demand. The amount of energy for additional heating in each case is given in Table 4.

It should be underlined that, for the specific case study with the given PV electricity production, only the UHT-TES unit can potentially utilize most of the available electricity from the PV when it operates under specific conditions (i.e. electricity priority – Case 2b) and for a minimum storage capacity of 40 kWh. In the rest of the cases, either a contract with the local DSO for grid injection or an additional battery for electricity storage is required.

Table 4: Basic energy-flow related annual parameters for each case

Parameters	Heat storage capacity (kWh)	Cases				
		Reference	1a	1b	2a	2b
Heat Coverage from Renewable (%)	3	15.31	14.97	20.14	11.24	4.69
	10		20.09	30.33	15.82	8.40
	40		23.74	45.76	22.09	11.53
Electricity Coverage from Renewable (%)	3	39.34	39.34	39.34	39.78	42.24
	10				40.41	45.74
	40				41.16	53.11
PV Usage (%)	3	53.40	57.51	54.25	58.68	60.98
	10		59.41	55.26	61.11	74.35
	40		60.61	56.95	63.59	99.62
Annual PV absorption (kWh)	3	9957	10724	10115	10941	11371
	10		11078	10304	11394	13864
	40		11301	10619	11857	18575
Additional heat consumption from source other than PV (kWh)	3	6311	6336	5951	6614	7103
	10		5955	5192	6273	6826
	40		5683	4042	5806	6592
Annual Electricity Grid consumption (kWh)	3	14799	14799	14799	14692	14093
	10				14540	13238
	40				14355	11439

4 Conclusions

Several cases of heating storage systems have been investigated in this study, aiming to determine their dynamic behavior and their performance in thermal and electric coverage and renewable energy

utilization of a given RES source. Investigation of dynamic behavior on hourly basis provides insight regarding the charging and discharging stages for the heat storage system cases as well as the sequence of energy absorption and supply from each system. Useful conclusions can be drawn from this investigation, such as the causes for increased or reduced heat and electricity coverage and PV absorption observed in each case, depending on the different method for converting electricity to thermal power. It has been shown that the cases which use an electric resistance present higher PV absorption percentages but lower heat and/or electricity coverage, in contrast to the cases that use a heat pump, which show the opposite behavior.

On the one hand, taking into account the energy flow analysis on a long-term scale (monthly and annual basis), it was concluded that the case with parallel coverage of both thermal and electric demands, optimized for electricity supply (Case 2b), is the most advantageous for electricity coverage in all circumstances. On the other hand, the most preferable case for heat supply is the one which includes both a heat pump and a heat storage system (Case 1b), albeit not providing any electricity. All the examined cases presented better performance than the reference one regarding PV usage. This allows to conclude that any case with heat storage is preferable for better exploiting the produced renewable energy than a conventional case without one. A lead is achieved when an ultra-high thermal energy storage is used for this purpose (Case 2). There is also a clear increasing dependency of heat and electric coverage and PV absorption with the increase of heat storage capacity. The implementation of this technology in the residential sector seems promising, since significant energy savings both in heat and electricity consumption can be achieved through the use of a proper configuration and strategy of such a storage system. All these facts make clear that UHT-TES technology has the potential of being a competitive storage option for domestic application and deserves further development towards this direction.

This study also presented that despite the adoption of such a storage system, heat and electricity demand cannot be fully covered exclusively from storage supply. This leaves room for further investigation and optimization, taking also into account parameters such as investment and operating costs, cost of electricity, energy savings, PV and heat battery capacity,etc.

5 Acknowledgements

This work has been carried out in the framework of the European Union's Horizon 2020 research and innovation programme under grant agreement No 731249 (SMart IsLand Energy Systems - SMILE) and the European Union's Horizon2020 research and innovation program, FET-OPEN action under grant agreement No 737054 (Next GenerAtion MateriAls and Solid State DevicEs for Ultra High Temperature Energy Storage and Conversion - AMADEUS). The sole responsibility for the content of this publication lies with the authors. It does not necessarily reflect the opinion of the European Union. Neither the REA nor the European Commission are responsible for any use that may be made of the information contained therein.

6 Nomenclature

A, m^2	inner tube wall area between two nodes i and i+1

$A_{abs,}$ m^2	absorber surface area of cylinder heat storage
$a_{HTF,i}$, W·m^{-2}·K^{-1}	convective heat transfer coefficient between the heat transfer fluid and the inner tube wall
c_p	Specific heat capacity of PCM
$c_{p,HTF}$, J·kg^{-1}K^{-1}	specific heat capacity of the heat transfer fluid
E, J	stored energy in the heat battery
E_{max}, J	maximum capacity of the heat battery
H, m	cylinder heat storage height
k_l, W·m^{-1}K^{-1}	thermal conductivity of liquid PCM
k_s, W·m^{-1}K^{-1}	thermal conductivity of solid PCM
L, J·kg^{-1}	PCM latent heat of fusion
$\dot{m}_{HTF}$, kg·s^{-1}	mass flow rate of the heat transfer fluid (here water)
P, W	electric power produced by the PV and input power in the heat battery from the electric resistance
Q, W	heat demand served by the heat battery
Q_e, *W*	heat flux at the emitter surface
$\dot{Q}_{HEX,i}$, W	heat flow transferred through the heat exchanger for each node i
$\dot{Q}_{tot}$, W	total heat flow transferred through the heat exchanger
R, Ω	electric resistance of the heat battery resistor
r_{in}, m	inner tube coil radius,
r_{out}, m	outer tube coil radius
r_{pcm}, m	half-distance between each pass of the tube-coil
SOC, -	state of charge of the heat battery
T_{em}, K	emitter temperature
$T_{HTF,in,i}$, K	temperature of the heat transfer fluid at node i
T_l, *K*	PCM melting point
T_{ref}, K	reference temperature
T_s, *K*	PCM solidification point
T_{pc}, K	phase change temperature of the PCM (58 °C)
$U_{HTF,i}$, W·m^{-2}·K^{-1}	overall heat transfer coefficient from HTF to PCM
V, V	voltage applied to the heat battery resistor
Greek letters	
$\Delta T_{ln,i}$, K	logarithmic mean temperature difference between HTF and PCM
λ_{Tc}, W·m^{-1}·K^{-1}	thermal conductivity of the tube coil (385 W/mK for copper)
λ_{eff}, W·m^{-1}·K^{-1}	effective thermal conductivity value of the PCM heat exchanger compound
$\lambda_{eff,l}$, W·m^{-1}·K^{-1}	effective thermal conductivity value of the PCM heat exchanger compound in liquid phase
$\lambda_{eff,s}$, W·m^{-1}·K^{-1}	effective thermal conductivity value of the PCM heat exchanger compound in solid phase
ρ_l, kg·m^{-3}	density of liquid PCM
ρ_s, kg·m^{-3}	Density of solid PCM

7 References

[1] J.S.f.P. Report, Energy Consumption and Energy Efficiency Trends in the EU-28 2000-2015, in, 2018.

[2] Clean energy for all Europeans package, in, European Commission, https://ec.europa.eu/energy/topics/energy-strategy/clean-energy-all-europeans_en, Published: 20 October 2017
[3] L. Murphy, Policy Instruments to Improve Energy Performance of Existing Owner Occupied Dwellings: Understanding and Insight, 2016.
[4] I.A. Atsonios, I.D. Mandilaras, D.A. Kontogeorgos, M.A. Founti, Two new methods for the in-situ measurement of the overall thermal transmittance of cold frame lightweight steel-framed walls, Energy and Buildings, 170 (2018) 183-194.
[5] I. Atsonios, I. Mandilaras, M. Founti, Thermal Assessment of a Novel Drywall System Insulated with VIPs, Energies, 12 (2019) 2373.
[6] J.C. Solano, L. Olivieri, E. Caamaño-Martín, Assessing the potential of PV hybrid systems to cover HVAC loads in a grid-connected residential building through intelligent control, Applied Energy, 206 (2017) 249-266.
[7] D. Mugnier, R. Fedrizzi, R. Thygesen, T. Selke, New Generation Solar Cooling and Heating Systems with IEA SHC Task 53: Overview and First Results, Energy Procedia, 70 (2015) 470-473.
[8] U. Eicker, A. Colmenar-Santos, L. Teran, M. Cotrado, D. Borge-Diez, Economic evaluation of solar thermal and photovoltaic cooling systems through simulation in different climatic conditions: An analysis in three different cities in Europe, Energy and Buildings, 70 (2014) 207-223.
[9] N. Hartmann, C. Glueck, F.P. Schmidt, Solar cooling for small office buildings: Comparison of solar thermal and photovoltaic options for two different European climates, Renewable Energy, 36 (5) (2011) 1329-1338.
[10] Y. Li, G. Zhang, G.Z. Lv, A.N. Zhang, R.Z. Wang, Performance study of a solar photovoltaic air conditioner in the hot summer and cold winter zone, Solar Energy, 117 (2015) 167-179.
[11] B.R. De Coninck R, Verbruggen B, Driesen J, Saelens D, Helsen L. , Modelling and simulation of a grid connected photovoltaic heat pump system with thermal energy storage using Modelica. , in: 8th Int Conf Syst Simul Build 2010, 2010, pp. 1-21.
[12] L. Bird, J. Cochran, X. Wang, Wind and solar energy curtailment: Experience and practices in the United States, in, National Renewable Energy Lab.(NREL), Golden, CO (United States), 2014.
[13] I. Dincer, M. Rosen, Thermal Energy Storage: Systems and Application; , Chichester, UK, 2011.
[14] A. Sharma, V.V. Tyagi, C.R. Chen, D. Buddhi, Review on thermal energy storage with phase change materials and applications, Renewable and Sustainable Energy Reviews, 13 (2) (2009) 318-345.
[15] A. Kumar, S.K. Shukla, A Review on Thermal Energy Storage Unit for Solar Thermal Power Plant Application, Energy Procedia, 74 (2015) 462-469.
[16] G. Hailu, Seasonal Solar Thermal Energy Storage, in: Thermal Energy Battery with Nano-enhanced PCM, IntechOpen, 2018.
[17] R. Waser, F. Ghani, S. Maranda, T.S. O'Donovan, P. Schuetz, M. Zaglio, J. Worlitschek, Fast and experimentally validated model of a latent thermal energy storage device for system level simulations, Applied Energy, 231 (2018) 116-126.
[18] K. Cellat, B. Beyhan, Y. Konuklu, C. Dündar, O. Karahan, C. Güngör, H. Paksoy, 2 years of monitoring results from passive solar energy storage in test cabins with phase change materials, Solar Energy, (2019).
[19] D.J. Malan, R.T. Dobson, F. Dinter, Solar Thermal Energy Storage in Power Generation Using Phase Change Material with Heat Pipes and Fins to Enhance Heat Transfer, Energy Procedia, 69 (2015) 925-936.
[20] B. Grange, C. Dalet, Q. Falcoz, A. Ferrière, G. Flamant, Impact of thermal energy storage integration on the performance of a hybrid solar gas-turbine power plant, Applied Thermal Engineering, 105 (2016) 266-275.

[21] J.F. Belmonte, M.A. Izquierdo-Barrientos, A.E. Molina, J.A. Almendros-Ibáñez, Air-based solar systems for building heating with PCM fluidized bed energy storage, Energy and Buildings, 130 (2016) 150-165.
[22] M.A. Izquierdo-Barrientos, C. Sobrino, J.A. Almendros-Ibáñez, Energy storage with PCM in fluidized beds: Modeling and experiments, Chemical Engineering Journal, 264 (2015) 497-505.
[23] M. Parsazadeh, X. Duan, Numerical and statistical study on melting of nanoparticle enhanced phase change material in a shell-and-tube thermal energy storage system, Applied Thermal Engineering, 111 (2017) 950-960.
[24] K. Kant, A. Shukla, A. Sharma, Performance evaluation of fatty acids as phase change material for thermal energy storage, Journal of Energy Storage, 6 (2016) 153-162.
[25] Z. Wang, H. Wang, X. Li, D. Wang, Q. Zhang, G. Chen, Z. Ren, Aluminum and silicon based phase change materials for high capacity thermal energy storage, Applied Thermal Engineering, 89 (2015) 204-208.
[26] A. Datas, A. Ramos, A. Martí, C. del Cañizo, A. Luque, Ultra high temperature latent heat energy storage and thermophotovoltaic energy conversion, Energy, 107 (2016) 542-549.
[27] A. Datas, M. Zeneli, C. del Cañizo, I. Malgarinos, A. Nikolopoulos, N. Nikolopoulos, S. Karellas, A. Martí, Molten silicon storage of concentrated solar power with integrated thermophotovoltaic energy conversion, AIP Conference Proceedings, 2033 (1) (2018) 090005.
[28] M. Zeneli, I. Malgarinos, A. Nikolopoulos, N. Nikolopoulos, P. Grammelis, S. Karellas, E. Kakaras, Numerical simulation of a silicon-based latent heat thermal energy storage system operating at ultra-high temperatures, Applied Energy, 242 (2019) 837-853.
[29] M. Zeneli, A. Nikolopoulos, A. Datas, N. Nikolopoulos, S. Karellas, E. Kakaras, Study of heat losses during charge, discharge and storage period of a LHTES system operating at ultra-high temperatures, in: ECOS Conference, Wroclaw, Poland, 2019.
[30] A. Datas, A.B. Cristobal, C. del Cañizo, E. Antolín, M. Beaughon, N. Nikolopoulos, A. Nikolopoulos, M. Zeneli, N. Sobczak, W. Polkowski, M. Tangstad, J. Safarian, D.M. Trucchi, A. Bellucci, M. Girolami, R. Marx, D. Bestenlehner, S. Lang, A. Vitulano, G. Sabbatella, A. Martí, AMADEUS: Next generation materials and solid state devices for ultra high temperature energy storage and conversion, AIP Conference Proceedings, 2033 (1) (2018) 170004.
[31] M.R. Reid, D.B. Scharfe, R.N. Webb, Computational evaluation of a latent heat energy storage system, Solar Energy, 95 (2013) 99-105.
[32] A. Datas, A. Ramos, C. del Cañizo, Techno-economic analysis of solar PV power-to-heat-to-power storage and trigeneration in the residential sector, Applied Energy, 256 (2019) 113935.
[33] V.R. Voller, P. C., A fixed grid numerical modelling methodology for convection-diffusion mushy region phase-change problems, Civil, Environmental, and Geo- Engineering, (1987).
[34] M. Zeneli, A. Bellucci, G. Sabbatella, D.M. Trucchi, A. Nikolopoulos, N. Nikolopoulos, S. Karellas, E. Kakaras, Performance evaluation and optimization of the cooling system of a hybrid thermionic-photovoltaic converter, Energy Conversion and Management, (2020).
[35] S. Quoilin, A. Desideri, J. Wronski, I. Bell, V. Lemort, ThermoCycle: A Modelica library for the simulation of thermodynamic systems, 2014.
[36] V. Gnielinski, On heat transfer in tubes, International Journal of Heat and Mass Transfer, 63 (2013) 134-140.
[37] I. Violidakis, M. Zeneli, K. Atsonios, G. Strotos, N. Nikolopoulos, S. Karellas, Dynamic modelling of an ultra high temperature PCM with combined heat and electricity production for application at residential buildings, Energy and Buildings, 222 (2020) 110067.
[38] A. Datas, Hybrid thermionic-photovoltaic converter, Applied Physics Letters, 108 (14) (2016) 143503.
[39] PVWatts Calculator, in, National Renewable Energy Laboratory, https://pvwatts.nrel.gov/

8 Annex

8.1 Heat Demand

Heat demand throughout a year, resulting from calculations based on the method of heating degree-hours for a typical South European residence is presented in Figure 17.

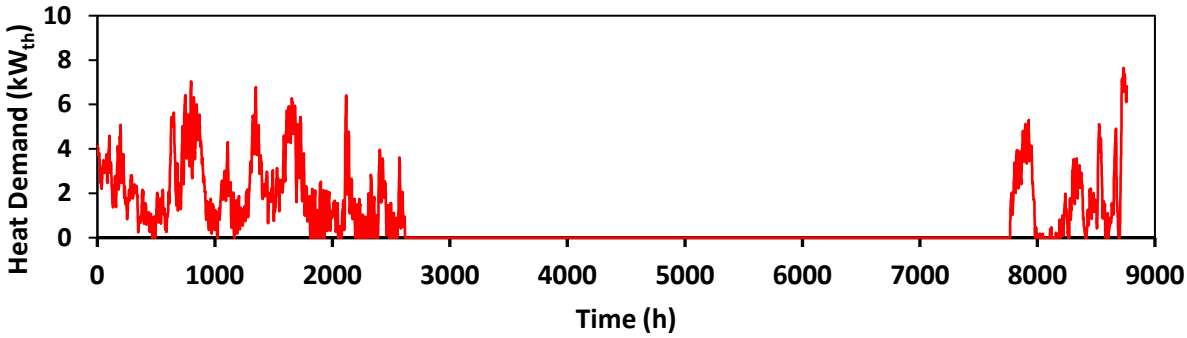

Figure 17. Heat demand throughout a year.

8.2 PV potential electric production

In all cases, production of electric energy is achieved through a PV which feeds the heating systems. The application of such a system in the specific area leads to an annual energy production profile as that of Figure 18, according to an online tool for providing location-based hourly power output from solar power plants [39]. Part of this electricity is led to cover directly the domestic electricity demand, and the remaining, excess PV potential electric production is shown in Figure 19.

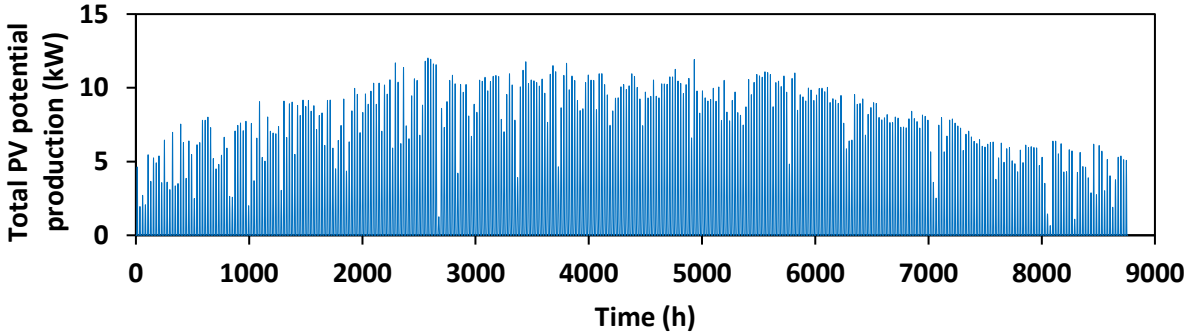

Figure 18. Typical electricity power production from a PV system installed in S. Europe throughout a year.

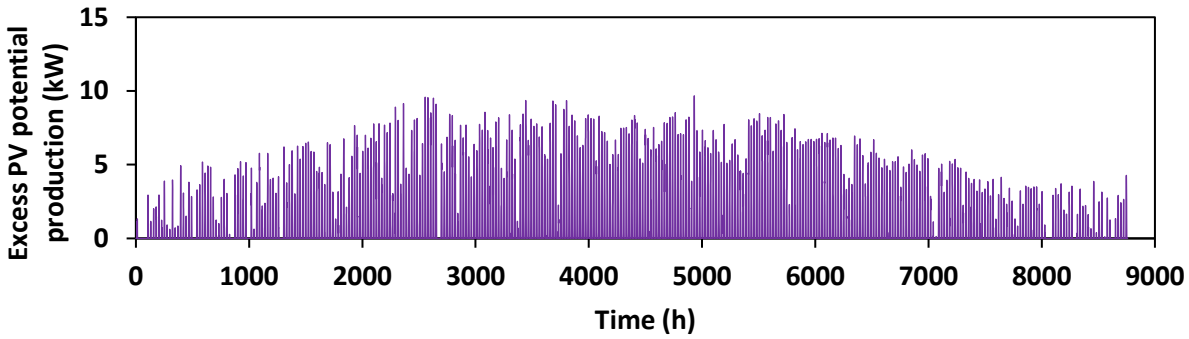

Figure 19. Excess electricity power production from a PV system.

8.3 Electricity Demand

For the electricity demand, a typical consumption profile of a south European residential building, as seen in Figure 20 has been considered. The PV covers part of this electrical demand directly, so the remaining demand after subtracting this already covered demand is shown in Figure 21.

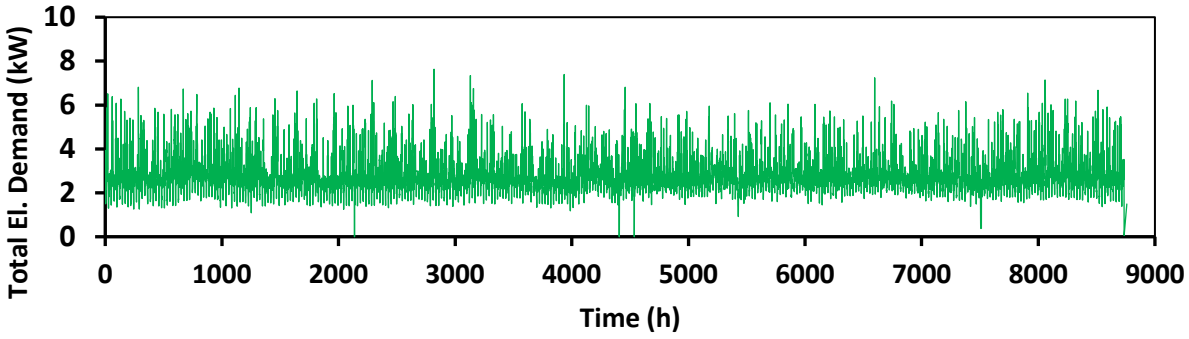

Figure 20. Electricity demand throughout a year.

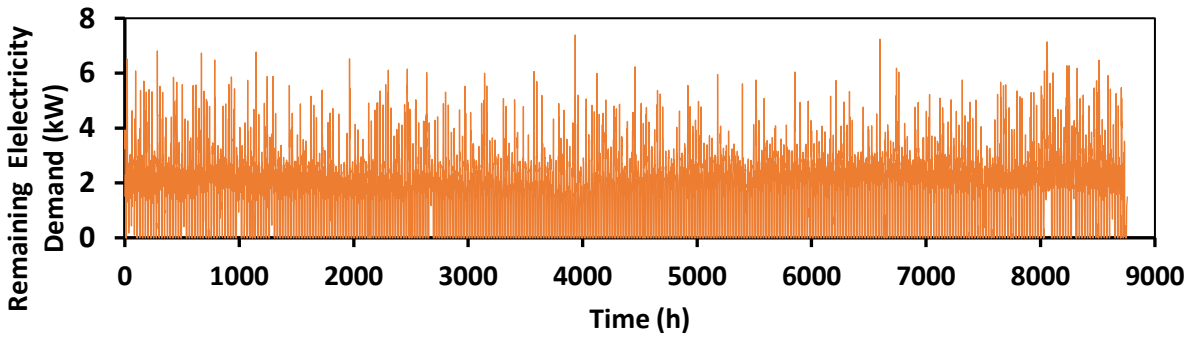

Figure 21. Remaining electricity demand throughout a year.